Formation of uniform magnetic structures and epitaxial hydride phases in Nd/Pr superlattices

J. P. Goff* and C. Bryn-Jacobsen
Oxford Physics, Clarendon Laboratory, Parks Road, Oxford OX1 3PU, United Kingdom

D. F. McMorrow
Department of Solid State Physics, Risø National Laboratory, DK-4000 Roskilde, Denmark

R. C. C. Ward and M. R. Wells
Oxford Physics, Clarendon Laboratory, Parks Road, Oxford OX1 3PU, United Kingdom

(Received 5 December 1996)

The chemical and magnetic structures of neodymium/praseodymium superlattices grown by molecular-beam epitaxy have been determined using x-ray and neutron-diffraction techniques. The x-ray measurements show that the superlattices have a dhcp structure of high crystalline quality, and that the stacking sequence is coherent over many bilayer repeats. The neutron measurements show that for the hexagonal sites of the dhcp structure, the Nd magnetic order propagates coherently through the Pr, whereas the order on the cubic sites is either suppressed or confined to single Nd blocks. It is also shown that the singlet ground state of Pr is perturbed to produce a local moment on the hexagonal sites, so that in some cases there is a uniform magnetic structure throughout the superlattice. These results cast new light on the theory of magnetic interactions in rare-earth superlattices. Within a few months of growth these light rare-earth samples are found to react with hydrogen to form new single-crystal phases, which are coherent with the epitaxial structure. [S0163-1829(97)05918-3]

I. INTRODUCTION

The magnetic properties of heavy rare-earth superlattices with the hexagonal close packed (hcp) crystal stucture have been studied extensively.[1–3] The most striking feature of these systems is the long-range coherence of the magnetic order over many bilayer repeats, even when electronically similar but nonmagnetic elements such as Y or Lu are one of the constituents of the superlattice. Here these investigations are extended to light rare-earth neodymium/praseodymium superlattices. These systems have several unique features which make them appealing to study. First, the localized $4f$ moments in bulk Nd form incommensurate structures with components of the modulation vectors in the basal plane, whereas bulk Pr has a nonmagnetic singlet ground state down to very low temperatures. Thus it is of interest to study whether in a superlattice the Nd magnetic order propagates coherently through the Pr by establishing a spin-density wave in the conduction band of the Pr, and whether the development of order in the Nd blocks affects the magnetism of the Pr ions. Secondly, the double hexagonal close-packed (dhcp) structure exhibited by the light rare earths has two inequivalent sites, of approximately cubic and hexagonal symmetry, and there is therefore the possibility that the magnetic order may propagate differently on the two sites. Thirdly, bulk Nd exhibits a variety of multi-q magnetic structures, and these may be modified in a superlattice.

Figure 1 shows the magnetic structure of bulk Nd. The magnetic moments on the hexagonal sites order in the basal plane below $T_N \sim$ 19.9 K with an antiferromagnetic coupling between hexagonal layers, and a longitudinal sinusoidal modulation in the $\boldsymbol{a}^*$ direction. As the temperature is lowered below $T \sim 19.1$ K the moments tilt away from $\boldsymbol{a}^*$ to give the so-called 2-q structure,[4] see Fig. 2(a). At temperatures below $T \sim 8.2$ K, ordering on the cubic sites occurs, and the magnetic moments adopt a 3-q structure and then, at temperatures below $T \sim 6$ K, there is a further transition to the 4-q structure shown in Fig. 2(b).[5] The moments on the cubic sites are along $\boldsymbol{a}$ directions and the modulation vectors differ from those associated with the hexagonal sites. In contrast Pr

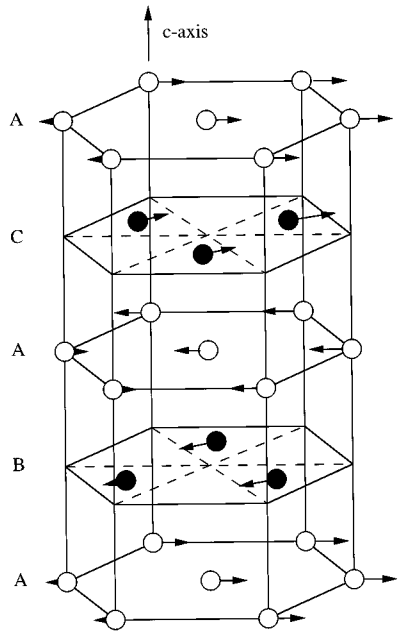

FIG. 1. The magnetic structure of bulk Nd. The hexagonal sites (filled circles) order at $T \sim 19.9$ K and the cubic sites (empty circles) order at $T \sim 8.2$ K.

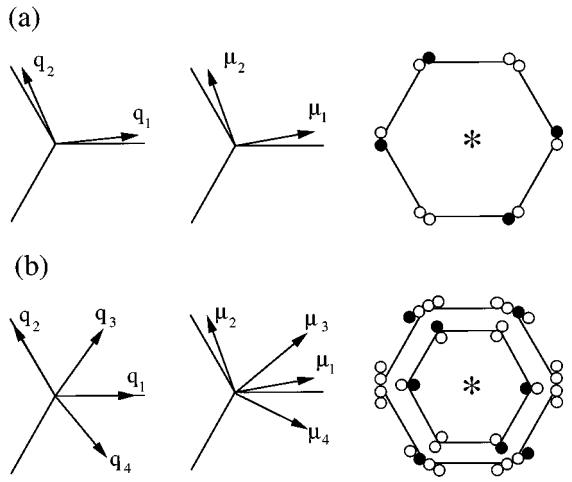

FIG. 2. Basal plane projections of modulation vectors, moment amplitudes, and the corresponding diffraction pattern around a nuclear Bragg point (*) (a) for the 2-q structure and (b) for the 4-q structure (Ref. 15). Filled circles result from the arrows shown, and unfilled circles arise from domain averaging.

has a singlet ground state and does not exhibit spontaneous long-range magnetic order until it is induced by the hyperfine coupling at $T \sim 0.05$ K, because the effect of the exchange interaction is insufficient to overcome the crystal-field splitting.[6] However, the hexagonal sites constitute an almost critical system and magnetic ordering may be induced by various perturbations.[7] When the Pr hexagonal sites order the magnetic structure closely resembles that of Nd just below its Néel temperature.

This paper describes studies of the chemical and magnetic structures of Nd/Pr superlattices. Section II describes the experimental techniques employed, and these comprise molecular-beam epitaxy (MBE) to grow the single-crystal superlattices, and x-ray and neutron diffraction in order to characterize their crystal and magnetic structures. The chemical structures are described in Sec. III, which includes a study of the reaction with hydrogen, and then the main results of the paper, the magnetic structures, are presented in Sec. IV. The observed magnetic ordering is discussed in terms of the theory of magnetic interactions in rare-earth superlattices in Sec. V, and finally some conclusions are drawn in Sec. VI.

II. EXPERIMENTAL TECHNIQUES

The single-crystal Nd/Pr superlattices were grown by MBE in the Balzers UMS 630 equipment at the Clarendon Laboratory[8] using growth techniques similar to those developed for heavy rare-earth superlattices.[9,10] A 1500 Å Nb buffer layer separates the rare earths from the sapphire substrate, and the superlattice structure is grown on top of a 1800 Å Y seed layer. In order to protect the light rare earths from reaction with the atmosphere the samples were capped with a 500 Å layer of Y. The epitaxial relationships in the growth direction are $\{1\,1\,0\}\ Al_2O_3 \parallel \{1\,1\,0\}\ Nb \parallel \{0\,0\,1\}$ Y, Nd/Pr. The close match between the Y, Nd, and Pr in-plane a lattice parameters facilitates the growth of an epitaxial structure of high crystalline quality. The optimum growth temperature, which limits interdiffusion at the interfaces, whilst still allowing sufficient surface mobility to promote layer-by-layer growth, depends primarily on the melting points of the constituents of the superlattice.[11] The melting points are close (Nd 1294 K; Pr 1234 K) so a growth temperature appropriate to both constituents can be chosen and, since they are significantly lower than those of the heavy rare earths, a lower growth temperature of 570 K was chosen. Nb, Y, and Pr were evaporated from electron-beam sources, and Nd from a Knudsen effusion cell, at a growth rate of 0.5 Å s^{-1}. The nominal structures are $Nd_{20}Pr_{20}$, $Nd_{33}Pr_{33}$, $Nd_{10}Pr_{30}$, $Nd_{30}Pr_{10}$, and $Nd_{40}Pr_{40}$, where the subscripts refer to the number of atomic planes in one bilayer, and the overall superlattice thickness was between 40 and 80 bilayer repeats.

The crystal quality of the epitaxial structures was determined using x-ray-diffraction techniques. The measurements were performed at room temperature at the Clarendon Laboratory using triple-crystal diffractometers and Cu $K\alpha$ radiation from a Stoe rotating anode source operating at 6 kW. The nature of the magnetic order was studied by neutron-diffraction techniques, using triple-axis spectrometers situated on the cold neutron source at Risø National Laboratory. The magnetic scattering from light rare-earth superlattices is weak due to the small volume of magnetic material ($\sim 10^{-4}$ cm^3) and the decreased moments in comparison to the heavy rare earths. An energy analyzer was used in order to separate the elastic magnetic diffraction from the inelastic background. The incident energy was fixed at $E = 4.95$ meV and higher-order contamination was suppressed using a beryllium filter. The instrumental collimation was chosen to give a wave-vector resolution of roughly 0.017 Å^{-1} in the scattering plane. Samples were cooled using a variable temperature cryostat, and measurements were taken over the temperature range $T = 2$–25 K.

III. CRYSTAL STRUCTURES

Table I summarizes the structural properties determined using x-ray-diffraction techniques. The mosaic spreads (0.1–$0.2°$) are relatively low for rare-earth superlattices, indicating that the samples are of high single-crystal quality. Figure 3(a) presents a typical scan of the wave-vector transfer $\boldsymbol{Q}$ along the [0 0 L] direction for the $Nd_{33}Pr_{33}$-I superlattice. Despite the small, one electron, x-ray-scattering contrast between the constituents, the superlattice peaks either side of the (004) Bragg reflection are clearly visible. The separation of the superlattice peaks gives the bilayer repeat distance, and the overall enveloping function provides details of the individual layer thicknesses and any interfacial roughness or interdiffusion. The data have been fitted to the structural model of Jehan *et al.*,[12] in which the number of planes n and the interplanar spacings d of each constituent are allowed to vary, and a tanh function is used to represent the variation of concentration and d spacing at the interfaces. The results are listed in Table I. The interplanar spacings are close to the bulk values $d_{Nd} \sim 2.951$ and $d_{Pr} \sim 2.960$ Å, and therefore the strains in these epitaxial structures are small. The fits also show that the interfaces extend over approximately four atomic planes, which is typical for rare-earth superlattices. Figure 4 presents the x-ray scattering observed

TABLE I. The structural parameters of the superlattices determined by fitting the model of Jehan *et al.* (Ref. 12), to the x-ray-diffraction data. $(Nd_{n_{Nd}}Pr_{n_{Pr}})_N$ is the nominal as-grown composition, with n_X the number of atomic planes of element X in one bilayer, N is the overall number of bilayers, d_X is the interplanar spacing, and λ is the extent of the interfacial region. The table also lists the measured single-crystal mosaic spreads.

Nominal structure	n_{Nd} ±2 planes	n_{Pr} ±2 planes	d_{Nd} ±0.003 Å	d_{Pr} ±0.003 Å	λ ±1 plane	Mosaic $\pm 0.03^o$
$(Nd_{20}Pr_{20})_{80}$-I	18	18	2.955	2.955	6	0.18
$(Nd_{30}Pr_{10})_{80}$-I	24	8	2.953	2.953	6	0.14
$(Nd_{10}Pr_{30})_{80}$-I	9	25	2.958	2.960	4	0.17
$(Nd_{20}Pr_{20})_{80}$-II	17	17	2.953	2.953	4	0.13
$(Nd_{33}Pr_{33})_{40}$-I	33	33	2.952	2.955	4	0.14
$(Nd_{40}Pr_{40})_{40}$-I	41	41	2.952	2.955	2	0.13
$(Nd_{33}Pr_{33})_{50}$-II	31	30	2.953	2.952	3	0.16
$(Nd_{20}Pr_{20})_{80}$-III	18	18	2.953	2.952	5	0.16
$(Nd_{10}Pr_{30})_{80}$-II	10	27	2.955	2.955	3	0.16

from $Nd_{10}Pr_{30}$-II for a scan of $\boldsymbol{Q}$ in the [1 0 L] direction which, unlike [0 0 L] scans, is sensitive to the positions of ions within the close-packed planes. Reflections are observed at the positions expected for the dhcp structure, and the fact that these peaks are narrow, and that superlattice reflections are observed, shows that the stacking sequence is coherent over at least 700 Å.

Measurements of the neutron scattering with a wave-vector transfer near the (004) structural reflection yield fits in agreement with those obtained using x rays. The neutron-scattering results when $\boldsymbol{Q}$ is scanned along the [0 0 L] direction for $Nd_{33}Pr_{33}$-I are presented in Fig. 3(b) for comparison with the x-ray data of Fig. 3(a). The neutron superlattice peaks are larger relative to the main Bragg reflection because of the greater scattering contrast between the constituents. Nevertheless the structural parameters were more accurately determined using the higher-intensity x-ray data.

Nd and Pr are more susceptible to reaction with the atmosphere than the heavy rare earths, and these superlattices were found to react to form new crystalline phases over a period of a few months. The x-ray measurements taken 120 days after growth for $Nd_{20}Pr_{20}$-I near the (004) reflection are presented in Fig. 5. Sharp new single-crystal Bragg reflections are observed, and these are located along the dhcp [0 0 L] and [1 0 L] axes, indicating that the new single-crystal phases are coherent with the original epitaxial structure. Further evolution of the x-ray scattering is shown for scans of $\boldsymbol{Q}$ along the [0 0 L] direction in Fig. 6, and [1 0 L] in Fig. 7. The triple-crystal diffraction results have been used in conjunction with the x-ray cylindrical camera technique[13] to identify the phases present at different times after growth, and these are listed in Table II.

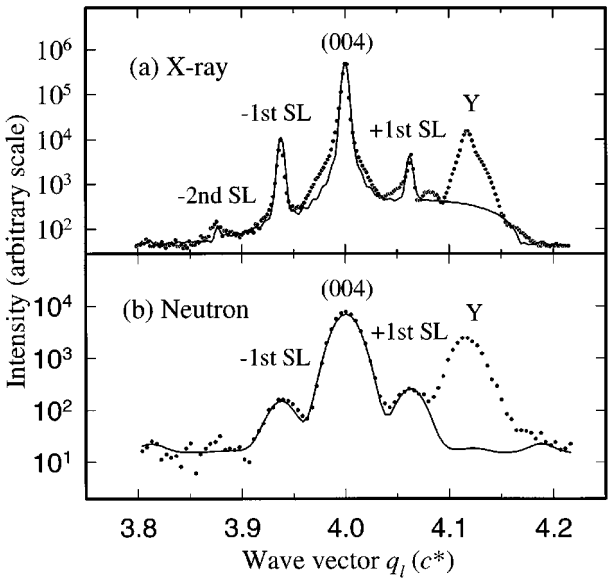

FIG. 3. Typical data for (a) x-ray, and (b) neutron, scans in the c^* direction for $Nd_{33}Pr_{33}$-I through the (0 0 4) Bragg peak, showing superlattice peaks on either side. The solid line shows a fit of structural parameters to the data, as discussed in the text.

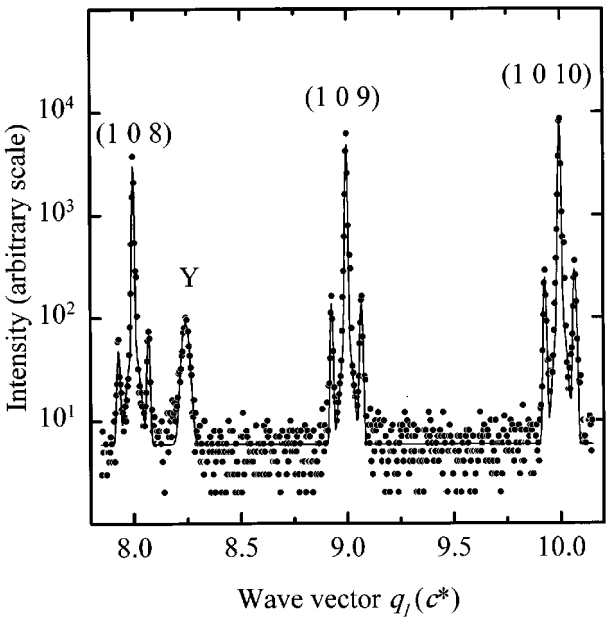

FIG. 4. The x-ray scattering observed for $\boldsymbol{Q}$ = (1 0 q_l) from $Nd_{10}Pr_{30}$-II, showing the coherence of the dhcp stacking sequence over many bilayer repeats.

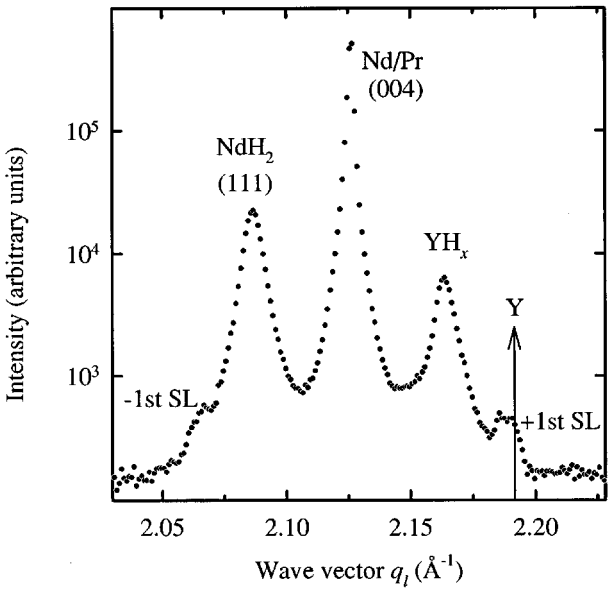

FIG. 5. The x-ray scattering observed from $Nd_{20}Pr_{20}$-I for $\boldsymbol{Q}=(0\ 0\ q_l)$ 120 days after growth, showing the (111) rare-earth hydride reflection, and the YH_x peak at a lower Q than for pure Y.

A similar reaction has been observed for thin films of yttrium, where capping with gold was found to catalyze the formation of hydrides and oxides.[14] In the case of the Nd/Pr system the reaction is likely to start at the edges of the superlattice, where Nd and Pr are exposed, rather than the top of the Y cap, which rapidly forms a protective oxide layer. It appears that hydrogen is able to diffuse through the rare-earth lattice without destroying the single crystals, and then the rare-earth close-packed planes are able to translate and change their stacking sequence, to form new epitaxial phases such as fcc-NdH_2. The hydrogen is then able to enter the Y seed and cap through the interfaces with the superlattice. The lattice expands as the concentration of hydrogen x in YH_x increases, so the Bragg reflections associated with Y move to lower $\boldsymbol{Q}$, see Fig. 5. The positions of the peaks in Figs. 6 and 7 are consistent with a change of structure to fcc-YH_2 after 140 days, and to YH_3 after 218 days. The Nd and Pr also react to form polycrystalline hydroxide as a loose powder. Eventually all of the dhcp Nd/Pr superlattice is lost, see Figs. 6 and 7. The Nb buffer layer is converted to epitaxial hydrides, but in this case the hydroxide is not formed.

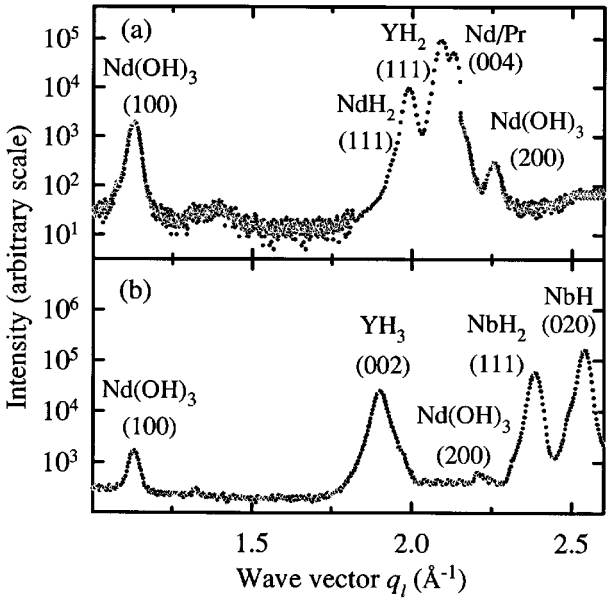

FIG. 6. The x-ray scattering observed from $Nd_{20}Pr_{20}$-I for $\boldsymbol{Q}=(0\ 0\ q_l)$ (a) 140 days and (b) 218 days after growth.

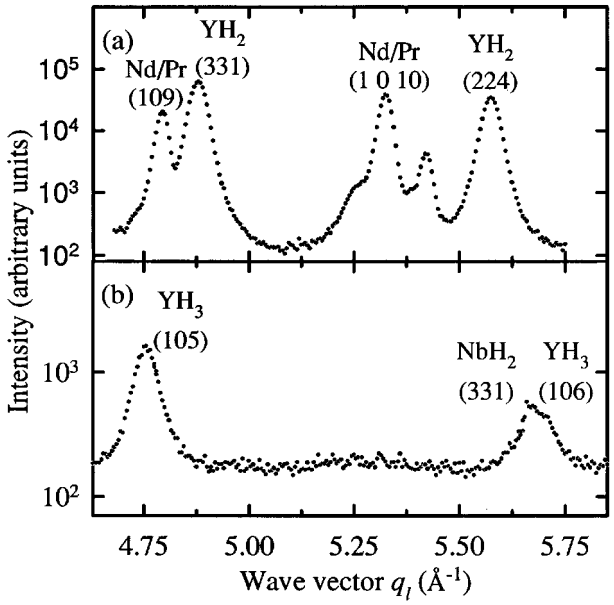

FIG. 7. The x-ray scattering observed from $Nd_{20}Pr_{20}$-I for $\boldsymbol{Q}=(1\ 0\ q_l)$ (a) 140 days and (b) 218 days after growth.

Fresh samples were grown for each new measurement of the magnetic properties, and these were checked for any signs of deterioration, such as reduction of the dhcp-Nd/Pr or hcp-Y intensities, or the appearance of hydride peaks. The neutron-diffraction studies of the magnetic ordering described in the next section were performed on unreacted superlattices with the dhcp structure.

IV. MAGNETIC STRUCTURES

For the samples with thicker layers, of nominal composition $Nd_{33}Pr_{33}$ and $Nd_{40}Pr_{40}$, the magnetic structures are found to be similar to that of bulk Nd. At temperatures below $T\sim 19$ K a peak in the scattering is observed for a wave-vector transfer $\boldsymbol{Q}=(q_h^{\rm hex}\ 0\ 3)$ where $q_h^{\rm hex}\sim 0.14$ reciprocal-lattice units (rlu) of the dhcp unit cell and, by analogy with bulk Nd, this is associated with magnetic ordering on the hexagonal sites. A further peak is observed at temperatures below 7 K for $\boldsymbol{Q}=(q_h^{\rm cub}\ 0\ 3)$ where $q_h^{\rm cub}\sim 0.19$, indicating ordering of the cubic sites. Figure 8(a) shows the results of scanning $\boldsymbol{Q}$ in the $\boldsymbol{a}^*$ direction through $(q_h\ 0\ 3)$ for $Nd_{33}Pr_{33}$-II at $T=2$ K. The temperature dependence of the scattering was determined in the $(h\ 0\ l)$ plane. The results of the projection of the ordering vector along $\boldsymbol{a}^*$ at $\boldsymbol{Q}=(q_h\ 0\ 3)$ for $Nd_{33}Pr_{33}$-II are compared with bulk Nd (Ref. 15) and a $Nd_{0.65}Pr_{0.35}$ alloy (Ref. 16) in Fig. 9. The coarse resolution perpendicular to the scattering plane (roughly 0.08 $Å^{-1}$) causes integration over any out of plane splitting of the peak (see Fig. 2). However, there is better resolution along the

TABLE II. The aging of the $Nd_{20}Pr_{20}$-I superlattice, with the phases identified using x-ray-diffraction techniques at different times after growth. The crystallographic axis parallel to the surface normal is given for the single-crystal hydride phases.

Age (days)	Phases	Axis	Comments
23	dhcp Nd/Pr	[001]	Same structure as grown
	hcp Y	[001]	
48	dhcp Nd/Pr	[001]	Same structure as grown
	hcp Y	[001]	
120	dhcp Nd/Pr	[001]	First signs of deterioration
	hcp Y	[001]	Y peak at lower Q
	fcc $(Nd,Pr)H_2$	[111]	
140	dhcp Nd/Pr	[001]	Reduced intensity of dhcp Nd/Pr
	fcc YH_2	[111]	No hcp Y
	fcc $(Nd,Pr)H_2$	[111]	Other unidentified phases
	hcp $Nd(OH)_3$	polycrystal	
218	hcp YH_3	[001]	No dhcp Nd/Pr
	fcc NbH_2	[111]	Other unidentified phases
	orthorhombic NbH	[010]	

$\boldsymbol{a}^*$ direction, and a longitudinal splitting of the $\boldsymbol{Q}=(q_h^{\rm hex}\ 0\ 3)$ peak is detected below $T=6$ K, as expected for the transition to the 4-q magnetic structure shown in Fig. 2(b).

In contrast, the behavior of the superlattices with thinner layers is found to be different from that of bulk Nd. For samples of nominal composition $Nd_{30}Pr_{10}$, $Nd_{20}Pr_{20}$ and $Nd_{10}Pr_{30}$ no cubic-site ordering is detected down to the lowest temperature measured, $T=2$ K. Furthermore, the longitudinal splitting of the hexagonal peak at $\boldsymbol{Q}=(q_h^{\rm hex}\ 0\ 3)$ is suppressed. Figure 8(b) shows a scan of $\boldsymbol{a}^*$ through $(q_h\ 0\ 3)$ for $Nd_{20}Pr_{20}$-I at $T=2$ K. Qualitatively similar behavior is observed in Nd:Pr alloys,[16–18], however since the x-ray results indicate minimal interdiffusion at the interfaces, this is a multilayer effect. The Néel temperatures for $Nd_{30}Pr_{10}$-I, $Nd_{20}Pr_{20}$-I, and $Nd_{10}Pr_{30}$-I are plotted as a function of Nd concentration in Fig. 10(a), and these are seen to fall as the

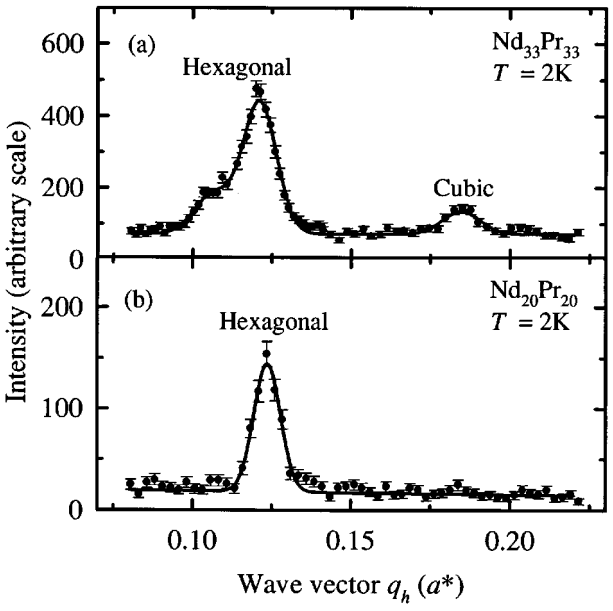

FIG. 8. The neutron scattering observed for $\boldsymbol{Q}=(q_h\ 0\ 3)$ at $T=2$ K from (a) $Nd_{33}Pr_{33}$-II and (b) $Nd_{20}Pr_{20}$-I. The cubic reflection and the longitudinal splitting of the hexagonal peak expected for the 4-q structure are observed for $Nd_{33}Pr_{33}$-II, but not for $Nd_{20}Pr_{20}$-I, which remains in the 2-q structure.

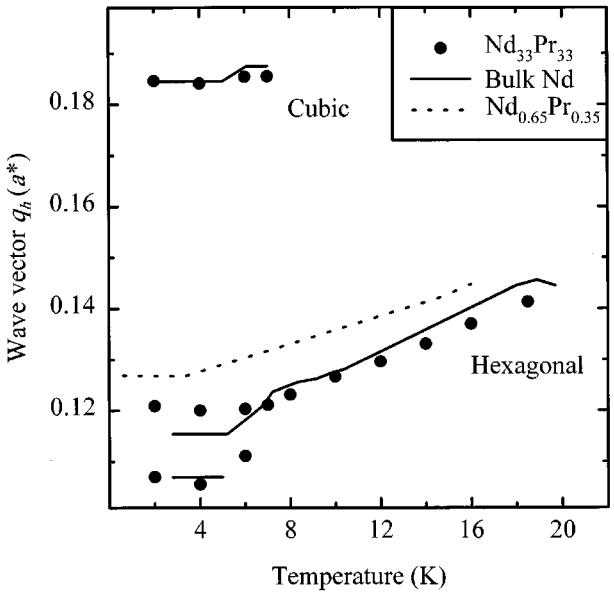

FIG. 9. The temperature dependence of the projection of the ordering wave vector along $\boldsymbol{a}^*$ for $\boldsymbol{Q}=(q_h\ 0\ 3)$ for $Nd_{33}Pr_{33}$-I. The results are compared with bulk Nd (solid lines) (Ref. 15) and a $Nd_{0.65}Pr_{0.35}$ alloy (dotted line) (Ref. 16). The Nd/Pr samples exhibit hysteresis, and these results were obtained by cooling from above T_N.

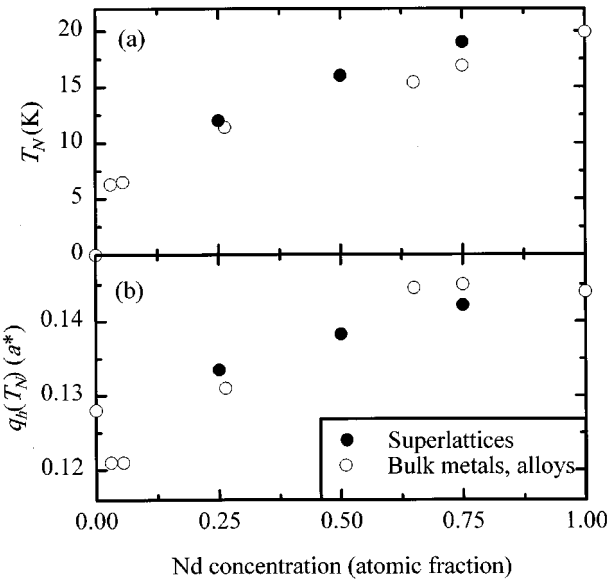

FIG. 10. The dependence of (a) the Néel temperature, T_N, and (b) the ordering wave vector at T_N, on the concentration of Nd for $Nd_{30}Pr_{10}$-I, $Nd_{20}Pr_{20}$-I, and $Nd_{10}Pr_{30}$-I superlattices compared with bulk metals (Refs. 6,15) and alloys (Refs. 16–18).

concentration of Nd decreases in a similar manner to the alloys. However, for a given concentration T_N tends to the bulk Nd value as the thickness of the Nd block increases. Figure 11 compares the results for q_h for the $Nd_{30}Pr_{10}$-I, $Nd_{20}Pr_{20}$I and $Nd_{10}Pr_{30}$-I superlattices with those for bulk Nd (Ref. 15) and a $Nd_{0.65}Pr_{0.35}$ alloy.[16] As the proportion of Pr increases the ordering wave vector at T_N decreases towards the value obtained for pure Pr,[6] similarly to the alloys, see Fig. 10(b). Measurements in the (h k 0) plane for

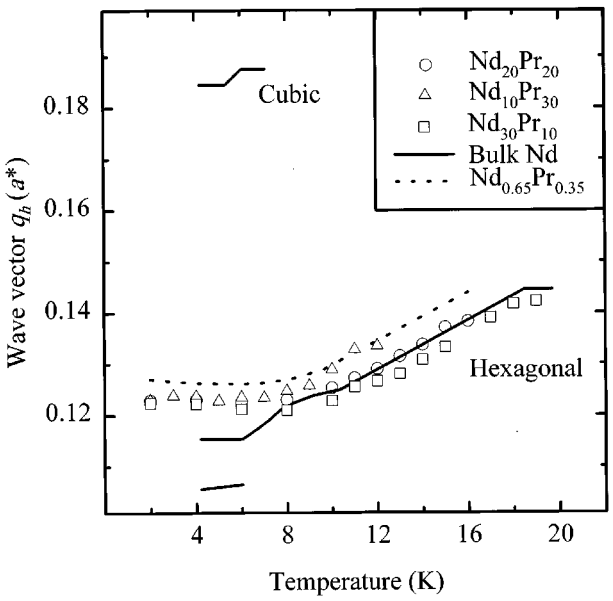

FIG. 11. The temperature dependence of the projection of the ordering wave vector along $\boldsymbol{a}^*$ for $\boldsymbol{Q}=(q_h\ 0\ 3)$ for $Nd_{20}Pr_{20}$-I, $Nd_{10}Pr_{30}$-I, and $Nd_{30}Pr_{10}$-I. The results are compared with bulk Nd (solid lines) (Ref. 15) and a $Nd_{0.65}Pr_{0.35}$ alloy (dotted line) (Ref. 16). These results were obtained on heating from $T\sim 2$ K.

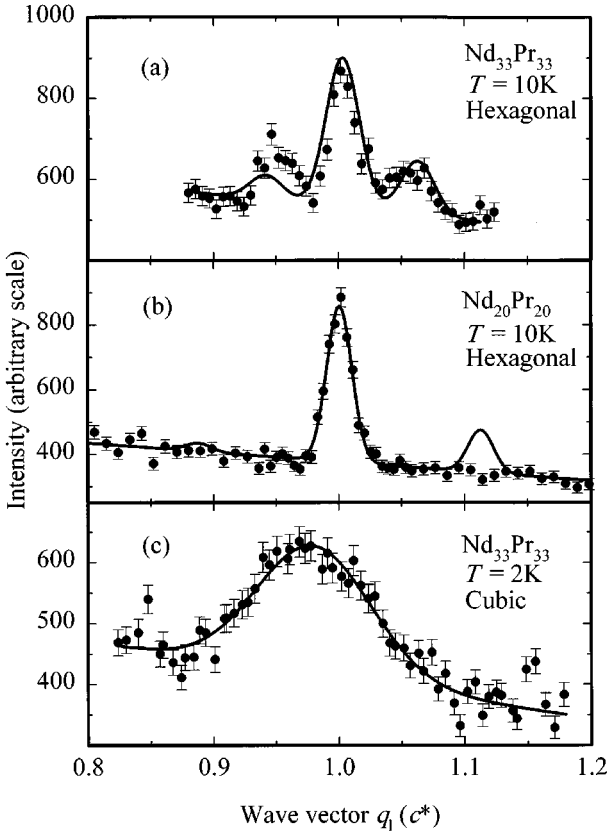

FIG. 12. Typical data from scans in the $\boldsymbol{c}^*$ direction through magnetic reflections. The scattering at $\boldsymbol{Q}=(q_h^{\rm hex}\ 0\ q_l)$ at $T=10$ K is shown (a) for $Nd_{33}Pr_{33}$-I, (b) for $Nd_{20}Pr_{20}$-II, and (c) at $\boldsymbol{Q}=(q_h^{\rm cub}\ 0\ q_l)$ at $T=2$ K for $Nd_{33}Pr_{33}$-II. The solid lines in (a) and (b) show calculations of the magnetic structure factors assuming no induced order in the Pr layers, and a fitted Gaussian profile in (c).

$Nd_{20}Pr_{20}$-I show a transverse splitting of the peak at $\boldsymbol{Q}=(1\ q_h^{\rm hex}\ 0)$ as expected for the 2-q structure [see Fig. 2(a)]. The magnitude of the splitting at $T=2$ K is 0.0045(5) rlu compared to 0.0054(1) rlu for $Nd_{0.65}Pr_{0.35}$ and zero for bulk Nd.

The scattering observed when $\boldsymbol{Q}$ is scanned in the $\boldsymbol{c}^*$ direction through magnetic reflections gives information on the magnetic ordering in the growth direction. Since the peak widths ΔQ corrected for instrumental resolution are related to the correlation lengths ξ through $\xi\sim 2\pi/\Delta Q$, they indicate whether the magnetic structure is coherent through the Pr layers, or if it is coherent only within single Nd blocks. The results also depend on whether order is induced in the Pr layers. If the magnetic order is coherent through the superlattice, and there is no magnetic moment on the Pr sites, magnetic superlattice reflections will be observed on either side of the average magnetic Bragg peak. However, if magnetic order is induced on Pr sites, there is a reduced magnetic moment contrast and the superlattice peak intensities decrease relative to the central peak. In the case of an identical magnetic structure and moment on the Nd and Pr sites the magnetic superlattice peaks are not observed.

The results of scanning $\boldsymbol{Q}$ in the $\boldsymbol{c}^*$ direction through the scattering at $\boldsymbol{Q}=(q_h^{\rm hex}\ 0\ 1)$ from $Nd_{33}Pr_{33}$-I for $T=10$ K are shown in Fig. 12(a). The widths of the peaks show that the magnetic order is coherent over many bilayer repeats. The

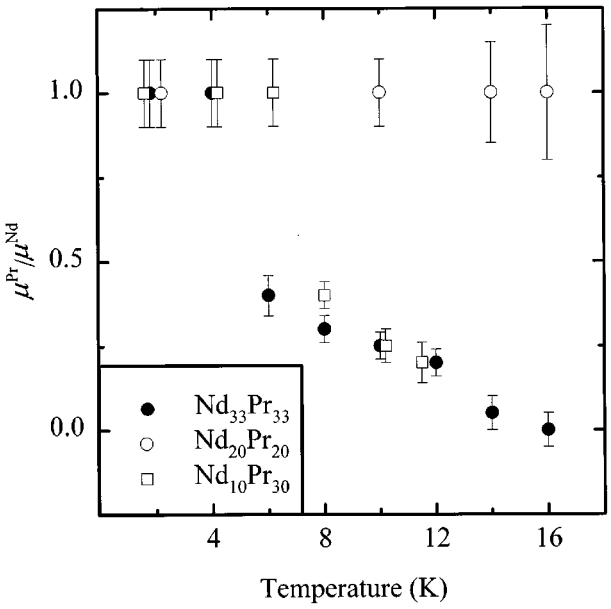

FIG. 13. Temperature dependence of the induced moment on Pr hexagonal sites determined from the magnetic superlattice intensities and the known epitaxial crystal structure, for $Nd_{33}Pr_{33}$-II, $Nd_{20}Pr_{20}$-III, and $Nd_{10}Pr_{30}$-II.

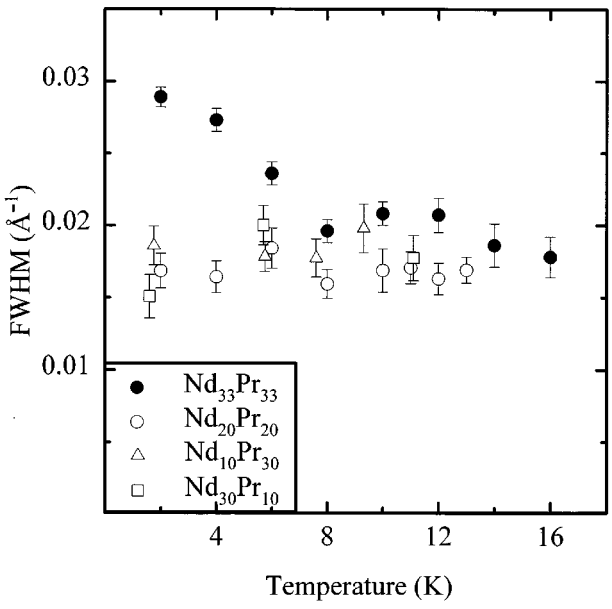

FIG. 14. Temperature dependence of the width of the magnetic Bragg reflection from the hexagonal sites in the $\boldsymbol{c}^*$ direction, for $Nd_{33}Pr_{33}$-II, $Nd_{20}Pr_{20}$-I, $Nd_{10}Pr_{30}$-I, and $Nd_{30}Pr_{10}$-I.

superlattice peaks on either side of the main peak clearly show the large moment contrast between the Nd and Pr layers. The same scan for $Nd_{20}Pr_{20}$-I is presented in Fig. 12(b), and this again shows that the magnetic order is coherent, but the absence of superlattice peaks indicates that order has been induced on the Pr hexagonal sites. Figures 12(a) and 12(b) also show the results of magnetic structure factor calculations for no induced moment in the Pr layers.

The relative amplitude of the induced Pr moment μ^{Pr}/μ^{Nd} may be obtained by comparing the intensities of the magnetic superlattice peaks with structure factor calculations using the known structural parameters and an antiferromagnetic arrangement of moments on the hexagonal sites. This is shown as a function of temperature in Fig. 13 for $Nd_{33}Pr_{33}$-II, $Nd_{20}Pr_{20}$-III, and $Nd_{10}Pr_{30}$-II. As the temperature is increased the Nd moment decreases, and for $Nd_{33}Pr_{33}$-II and $Nd_{10}Pr_{30}$-II the induced moment in the Pr falls until it is negligible close to the Néel temperature. However, when the temperature is reduced to $T\sim 4$ K, there is an abrupt increase in the induced moment, and the moment ratio becomes equal to unity. The Pr hexagonal sites in $Nd_{20}Pr_{20}$-III have the same moments as the Nd sites for all temperatures studied, and this sample therefore appears to exhibit a uniform magnetic structure over both constituents of the superlattice. For these thin-film samples the magnetic domains are not found to be randomly populated and, therefore, it is not possible to determine the absolute moment from measurements in the $(h\ 0\ l)$ plane.

The temperature dependence of the widths of the hexagonal magnetic Bragg peak in the $\boldsymbol{c}^*$ direction are shown in Fig. 14 for $Nd_{33}Pr_{33}$-II, $Nd_{20}Pr_{20}$-I, $Nd_{10}Pr_{30}$-I, and $Nd_{30}Pr_{10}$-I. The peak remains resolution limited at all temperatures for $Nd_{20}Pr_{20}$-I, $Nd_{10}Pr_{30}$-I, and $Nd_{30}Pr_{10}$-I, implying that the correlation length in the growth direction is greater than 800 Å, and that the magnetic structure is coherent over many bilayer repeats. Although there is some broadening for the thicker $Nd_{33}Pr_{33}$-II sample, there is found to be coherence over several bilayer repeats at all temperatures measured, whether or not the Pr sites are ordered. A broadening of the hexagonal peak in $Nd_{33}Pr_{33}$-II occurs below $T=7$ K, and this is possibly correlated with the onset of order on the cubic sites. No broadening is detected for $Nd_{10}Pr_{30}$-I which has a similar Pr thickness, but does not develop order on the cubic sites. For $Nd_{40}Pr_{40}$-I the hexagonal peak is considerably broader at all temperatures, and the correlation length ξ corresponds to about one bilayer thickness, suggesting that the hexagonal order loses coherence if there are 40 or more atomic planes of Pr.

The coherence of the cubic sites was studied by scanning $\boldsymbol{Q}$ in the $\boldsymbol{c}^*$ direction through $\boldsymbol{Q}=(q_h^{cub}\ 0\ 1)$ for $Nd_{33}Pr_{33}$-II at $T=2$ K. The scattering follows a broad Gaussian, see Fig. 12(c). After correction for instrumental resolution, the width corresponds to a correlation length $\xi\sim 110$ Å, which is comparable to one Nd block thickness. The cubic peak for $Nd_{40}Pr_{40}$-I was also found to be broad. Thus the magnetic order on the cubic sites is confined to individual Nd blocks, unlike that on the hexagonal sites.

V. MAGNETIC INTERACTIONS

There has recently been extensive discussion of the mechanisms responsible for the propagation of magnetic order between magnetic regions through an intermediate layer in metallic multilayers.[7,19–22] For rare-earth superlattices there is general agreement that, whether or not this intermediate layer is magnetic, the conduction electrons provide the necessary coupling, through the medium of a spin-density wave. However, there are differing views about the relative

importance of the nonlocal magnetic response of the intermediate layer, as manifested in the static susceptibility $\chi(\boldsymbol{q})$, and the matching of the wave functions and the band structures which occurs at the interface. According to the first view, the essential element in determining the propagation through the intermediate layer is its large conduction-electron susceptibiliy at the appropriate wave vector, whereas the second ascribes primary importance to the matching of the Fermi surfaces, which results in a lowering of the energy due to the smooth propagation of the spin-density wave through the interface.

It is difficult to distinguish experimentally between these two mechanims since systems with similar Fermi surfaces also usually have suitable peaks in $\chi(\boldsymbol{q})$. Nevertheless the results described here for Nd/Pr superlattices have implications for these theories. Although the measured magnetic excitation spectra of Pr metal provide evidence for a susceptibility of the conduction electrons that is large for an antiferromagnetic configuration of the hexagonal layers and small for cubic site ordering,[7] there is no evidence for exchange between hexagonal sites extending over 33 atomic planes, as found in our study. The Fermi surface-matching mechanism can account for coherence on the hexagonal sites in the superlattices since the magnetic structures of the bulk samples are similar at the ordering temperature. It also readily explains the lack of coherence in Nd/Y (Ref. 23) and Ho/Pr (Ref. 24) hcp/dhcp superlattices. However, this model has to ascribe the absence of coherent ordering on the cubic sites in Nd/Pr superlattices to Fermi surfaces which are congruent in one region but not another. Thus, further theoretical studies of the electronic structures in rare-earth superlattices are required.

In bulk Pr it is found that magnetic order may be induced on the hexagonal sites by the application of a uniaxial pressure[25] or an external magnetic field,[26] or by alloying with a small concentration of Nd ions.[6] However, these mechanisms are unlikely to be responsible for the induced ordering reported here for Nd/Pr superlattices. The x-ray structural studies show that any alloying is confined to a region close to the interfaces and that the epitaxial strains are small. Further evidence that strain is not responsible is provided by neutron-scattering measurements on a comparable system, a thin film of Pr grown on an Y seed layer, where no magnetic order was observed above $T \sim 0.11$ K.[27] Instead it is possible that the establishment of the conduction-electron spin-density wave in the Pr layers alters the effects of the exchange sufficiently to outweigh the crystal-field splitting and induce spontaneous order. The fact that the induced moment is comparable to the Nd moment is reasonable since the theoretical saturation moments $gJ\mu_B$ are 3.27 and $3.20\mu_B$ for Nd and Pr, respectively.

Incorporation of Pr in a superlattice structure gives a higher induced ordering temperature (above 10 K) than has hitherto been observed, and provides the first clear experimental evidence for Pr in the 2-q magnetic structure. Furthermore the Pr hexagonal sites follow the same temperature dependence for their ordering wave vectors as the Nd. We intend to study the induced order in the Pr layers further at an x-ray synchrotron source using resonance-enhanced magnetic scattering, where it is possible to distinguish between polarization of the $5d$ bands and ordering of $4f$ moments on Pr sites.

VI. CONCLUSIONS

In summary, we have carried out the first studies of superlattices in which both components are light rare-earth metals, and have observed a number of new phenomena. Nd/Pr superlattices show very different magnetic behavior on their hexagonal and cubic sites. The hexagonal order is coherent over many bilayers, but the cubic order is confined to individual Nd blocks. Furthermore, the development of this cubic order appears to reduce the range of coherence of the hexagonal ordering. Order may be induced on the Pr hexagonal sites so that in some cases the two constituents of the superlattice exhibit a uniform magnetic structure. These results provide important information on the magnetic interactions in metallic superlattices. We have also discovered that these superlattices react with hydrogen to form epitaxial single-crystal phases.

ACKNOWLEDGMENTS

We would like to express our gratitude to R. A. Cowley for his help and advice, and to A. R. Mackintosh and B. Lebech for many useful discussions. The expert technical assistance of the staff of Risø National Laboratory is gratefully acknowledged. Financial support was provided by the EPSRC in the UK, and by the EU under its Large Scale Facilities Programme in Denmark.

*Author to whom correspondence should be addressed. FAX: 44-1865-272400; Electronic address: GOFF@PH.OX.AC.UK

[1] M. B. Salamon, S. Sinha, J. J. Rhyne, J. E. Cunningham, R. W. Erwin, J. A. Borchers, and C. P. Flynn, Phys. Rev. Lett. **56**, 259 (1986).

[2] C. F. Majkrzak, J. Kwo, M. Hong, Y. Yafet, D. Gibbs, C. L. Chien, and J. Bohr, Adv. Phys. **40**, 99 (1991).

[3] R. A. Cowley, D. F. McMorrow, J. A. Simpson, D. A. Jehan, P. P. Swaddling, R. C. C. Ward, and M. R. Wells, J. Appl. Phys. **76**, 6274 (1994).

[4] K. A. McEwen, E. M. Forgan, H. B. Stanley, J. Bouillot, and D. Fort, Physica B **130**, 360 (1985).

[5] E. M. Forgan, E. P. Gibbons, K. A. McEwen, and D. Fort, Phys. Rev. Lett. **62**, 470 (1989).

[6] H. Bjerrum Møller, J. Z. Jensen, M. Wulff, A. R. Mackintosh, O. D. McMasters, and K. A. Gschneider Phys. Rev. Lett. **49**, 482 (1982).

[7] J. Jensen and A. R. Mackintosh, *Rare Earth Magnetism* (Oxford University Press, New York, 1991).

[8] R. C. C. Ward, M. R. Wells, C. Bryn-Jacobsen, R. A. Cowley, J. P. Goff, D. F. McMorrow, and J. A. Simpson, Thin Solid Films **275**, 137 (1996).

[9] S. M. Durbin, J. E. Cunningham, and C. P. Flynn, J. Phys. F **12**, L75 (1982).

[10] J. Kwo, E. M. Gyorgy, D. B. McWhan, M. Hong, F. J. Disalvo, C. Vettier, and J. E. Bower, Phys. Rev. Lett. **55**, 1402 (1985).

[11] C. P. Flynn, J. Phys. F **18**, L195 (1988).

[12] D. A. Jehan, D. F. McMorrow, R. A. Cowley, R. C. C. Ward, M.

R. Wells, N. Hagmann, and K. N. Clausen, Phys. Rev. B **48** 5594 (1993).
[13] C. A. Wallace and R. C. C. Ward J. Appl. Crystallogr. **8**, 255 (1975).
[14] A. R. Wildes, R. C. C. Ward, M. R. Wells, and B. Hjorvarsson J. Alloys Compounds **242**, 49 (1996).
[15] B. Lebech, J. Wolny, and R. M. Moon, J. Phys. Condens. Matter **6**, 5201 (1994).
[16] J. Wolny and B. Lebech, J. Magn. Magn. Mater. **140-144**, 741 (1995).
[17] B. Lebech, K. A. McEwen, and P. A. Lingard, J. Phys. C **8**, 1684 (1975).
[18] K. A. McEwen, B. Lebech, and D. Fort, J. Magn. Magn. Mater. **54-57**, 457 (1986).
[19] J. J. Rhyne, R. W. Erwin, J. Borchers, S. Sinha, M. B. Salamon, R. Du, and C. P. Flynn J. Appl. Phys. **61**, 4043 (1987).
[20] Y. Yafet, J. Kwo, M. Hong, C. F. Majkrzak, and T. O'Brien, J. Appl. Phys. **63**, 3453 (1988).
[21] J. A. Simpson, D. F. McMorrow, R. A. Cowley, D. A. Jehan, R. C. C. Ward, M. R. Wells, and K. N. Clausen, Phys. Rev. Lett. **73**, 1162 (1994).
[22] B. Heinrich and J. F. Cochran, Adv. Phys. **42**, 523 (1993).
[23] B. A. Everitt, J. A. Borchers, M. B. Salamon, J. J. Rhyne, R. W. Erwin, B. J. Park, and C. P. Flynn, J. Magn. Magn. Mater. **140-144**, 769 (1995).
[24] J. A. Simpson, D. F. McMorrow, R. A. Cowley, R. C. C. Ward, and M. R. Wells, J. Phys. Condens. Matter **7**, L417 (1995).
[25] K. A. McEwen, W. G. Stirling, and C. Vettier, Phys. Rev. Lett. **41**, 343 (1978).
[26] K. A. McEwen, G. J. Cock, L. W. Roeland, and A. R. Mackintosh, Phys. Rev. Lett. **30**, 287 (1973).
[27] J. P. Goff, C. Bryn-Jacobsen, D. F. McMorrow, J. Jensen, G. J. McIntyre, J. A. Simpson, R. A. Cowley, R. C. C. Ward, and M. R. Wells (unpublished).